Supramolecular Engineering of Cathode Materials for Aqueous Zinc-ion Energy Storage Devices: Novel Benzothiadiazole Functionalized Two-Dimensional Olefin-Linked COFs

Haijun Peng, Senhe Huang, Verónica Montes Garcia, Dawid Pakulski, Haipeng Guo, Fanny Richard, Xiaodong Zhuang, Paolo Samorì, Artur Ciesielski

How to cite: *Angew. Chem. Int. Ed.* **2023,** *62,* e202216136
International Edition: doi.org/10.1002/anie.202216136
German Edition: doi.org/10.1002/ange.202216136

Zn-Ion Batteries

Supramolecular Engineering of Cathode Materials for Aqueous Zinc-ion Energy Storage Devices: Novel Benzothiadiazole Functionalized Two-Dimensional Olefin-Linked COFs

Haijun Peng, Senhe Huang, Verónica Montes-García, Dawid Pakulski, Haipeng Guo, Fanny Richard, Xiaodong Zhuang, Paolo Samorì, and Artur Ciesielski**

Abstract: Two-dimensional covalent organic frameworks (COFs) have emerged as promising materials for energy storage applications exhibiting enhanced electrochemical performance. While most of the reported organic cathode materials for zinc-ion batteries use carbonyl groups as electrochemically-active sites, their high hydrophilicity in aqueous electrolytes represents a critical drawback. Herein, we report a novel and structurally robust olefin-linked COF-TMT-BT synthesized via the aldol condensation between 2,4,6-trimethyl-1,3,5-triazine (TMT) and 4,4′-(benzothiadiazole-4,7-diyl)dibenzaldehyde (BT), where benzothiadiazole units are explored as novel electrochemically-active groups. Our COF-TMT-BT exhibits an outstanding Zn^{2+} storage capability, delivering a state-of-the-art capacity of 283.5 mAh g^{-1} at 0.1 A g^{-1}. Computational and experimental analyses reveal that the charge-storage mechanism in COF-TMT-BT electrodes is based on the supramolecularly engineered and reversible Zn^{2+} coordination by the benzothiadiazole units.

[*] Dr. H. Peng, Dr. V. Montes-García, Dr. H. Guo, Dr. F. Richard, Prof. P. Samorì, Dr. A. Ciesielski
Université de Strasbourg, CNRS, Institut de Science et d'Ingénierie Supramoléculaires
8 allée Gaspard Monge, 67000 Strasbourg (France)
E-mail: ciesielski@unistra.fr
samori@unistra.fr

S. Huang, Prof. X. Zhuang
The Soft2D Lab, State Key Laboratory of Metal Matrix Composites, Shanghai Key Laboratory of Electrical Insulation and Thermal Ageing, School of Chemistry and Chemical Engineering, Shanghai Jiao Tong University
200240, Shanghai (China)

Dr. D. Pakulski, Dr. A. Ciesielski
Centre for Advanced Technologies, Adam Mickiewicz University
Uniwersytetu Poznańskiego 10, 61-614 Poznań (Poland)
and
Adam Mickiewicz University Foundation
Poznań Science and Technology Park Rubież 46, 61-612 Poznań (Poland)

Introduction

In 2021, the price of lithium carbonate, the mineral precursor of lithium compounds used in lithium-ion batteries, skyrocketed by 500 % as a direct consequence of the demand boom for powering electric vehicles as well as the increasing shortage of lithium, which has been listed as critical raw material in 2020. Among the monovalent (Li^+, Na^+, and K^+) and multivalent metal-ion (Ca^{2+}, Mg^{2+}, Zn^{2+} and Al^{3+}) batteries, rechargeable aqueous zinc-ion batteries (ZIBs) represent the most promising alternative for large-scale energy storage devices owing to their inherent safety, environmental sustainability, and relatively low cost.[1] Despite these merits, most common cathode materials (i.e., metal oxides) still present several critical barriers which impede the widespread use of rechargeable ZIBs. The structure instability due to the crystal lattice evolution energy, structural strain and irreversible dissolution during the Zn^{2+} insertion process results in poor cyclability and low coulombic efficiency. Moreover, the typically employed cathode materials, i.e., V_2O_5,[2] MnO_2,[3] MoO_3,[4] and Prussian-blue analogues (PBA),[5] also represent a potential environmental threat. Fortunately, the above limitations can be overcome by developing novel cathode materials.[6] Covalent organic frameworks (COFs) represent an emerging class of porous crystalline polymers with high thermal and chemical stability owing to the nature of their architectures in which small molecular units are linked via covalent bonds.[7] COFs are attracting increasing interest in the field of energy-storage due to their intrinsically unique features including structural hence functional diversity as a result of their tuneable chemical structures, high porosity, and large internal surface areas.[8] Their crystalline structure and planarity can also be tuned to boost their electrochemical performance. In particular, planar COFs that present a AA stacking pattern represent the ideal candidates to allow continuous ion (e.g., Zn^{2+}) diffusion, thereby facilitating the access to the specific active sites.[9] Importantly, the use of electrochemically-active building blocks has proven to be the key to the realization of the next generation of high-performance electrode materials for energy storage applications.[10] Altogether, these features make COFs potentially promising cathode materials for rechargeable aqueous ZIBs. In 2019, Banerjee et al., reported for the first time the use of a classical two-dimensional (2D)-COF HqTp as a cathode material for rechargeable aqueous ZIBs,

delivering a specific capacity of 276.0 mAh g^{-1} at 0.125 A g^{-1}.[11] Other examples of COFs used as cathode materials in aqueous ZIBs exhibiting a high electrochemical performance include a 2D polyarylimide COF (capacity 92 mAh g^{-1} at 0.7 A g^{-1}) reported by Feng et al.,[12] an orthoquinone COF (225 mAh g^{-1} at 0.1 A g^{-1}) reported by Chen et al.,[13] and phenanthroline and quinone COF (247 and 344 mAh g^{-1} at 0.1 A g^{-1}) reported by Alshareef et al.[14] Hitherto, the majority of the COFs explored in energy applications are constructed via dynamic covalent bonds (e.g., imine bonds), and despite of being highly crystalline materials, they usually lack in-plane π-conjugation that can facilitate charge transport and they exhibit low stability in aqueous electrolytes, limiting their long-term cyclability. Therefore, COFs based on irreversible covalent carbon-carbon double bonds (–C=C–) are highly sought after for real applications. On the other hand, most of the electrochemically-active cathode materials in rechargeable aqueous ZIBs, not only based on COFs but also on other organic materials including polymers (e.g., PDA,[15] CLPy,[16]) and small organic molecules (e.g., small quinones such as TABQ[17] calix[4]quinones (C4Q),[18] triangular (PQ-D)[19] and heterocyclic (DTT)[20] quinones TABQ, tetracholoro-1,4-benzoquinone,[21] phenothiazine,[22]), use carbonyl (C=O) moieties as electrochemically-active groups to reversibly coordinate Zn^{2+}. However, the high hydrophilicity of organic carbonyl materials in aqueous electrolytes leads to parasitic side reactions and to the growth of zinc dendrites, which yields in reduced electronic conductivity and discharge potential, altogether representing critical drawbacks for their energy applications.[23]

In addition to the prevailing carbonyl derivatives, other electrochemically-active groups, including those containing N-based bonds[24] and S-based bonds,[25] have gained considerable attention, and provided enhanced electrochemical performance. Nitrogen and sulfur atoms, exhibit a higher electronegativity (3.04 and 2.58, respectively) compared to that of carbon (2.55), and as a result their addition to a carbon-based material's lattice improves not only its electrical conductivity but also the electrochemical performance. Thiadiazole derivatives, that contain both nitrogen and sulfur atoms have been used as cathode materials for rechargeable lithium batteries, exhibiting a dramatically improved performance.[26] Besides, benzothiadiazole has been widely used as effective electron-accepting unit for high-performance field-effect transistors (FETs).[27] However, to the best of our knowledge, they have not been employed as building blocks in COFs for energy applications.

In this work, we report a novel benzothiadiazole-functionalized olefin-linked COF, i.e., COF-TMT-BT, generated via the aldol condensation of 2,4,6-trimethyl-1,3,5-triazine (TMT) and 4,4′-(benzothiadiazole-4,7-diyl)dibenzaldehyde (BT). COF-TMT-BT comprises irreversible C=C linkages rendering it insoluble in aqueous-based electrolytes and it contains benzothiadiazoles as electrochemically-active groups. An aqueous ZIB is assembled, in which COF-TMT-BT and Zn foil are used as cathode and anode, respectively, while an aqueous solution containing zinc trifluoromethanesulfonate ($Zn(CF_3SO_3)_2$) serves as electrolyte. Density functional theory (DFT) simulations together with in situ Fourier-transform infrared spectroscopy analysis and ex situ X-ray photoelectron spectroscopy analysis, demonstrated that the electrochemically-active benzothiadiazole units coordinate the Zn^{2+} governing the mechanism of ion storage and release by taking advantage of the supramolecular nature of the reversible bond. COF-TMT-BT-based ZIB displayed a specific capacity of 283.5 mAh g^{-1} at a current density of 0.1 A g^{-1} as well as an outstanding maximum energy density of 219.6 Wh kg^{-1} and power densities of 23.2 kW kg^{-1}, which, according to our knowledge, are superior to most of the reported COFs cathodes and another organic or inorganic electrode materials to date. These findings not only highlight the importance of the rational design of novel electrochemically-active COFs but also offers an efficient strategy to construct high-performance cathodes for aqueous ZIBs. Moreover, both nitrogen and sulfur atoms are highly suitable for hosting, through reversible non-covalent interactions, monovalent and bivalent cations, offering an additional control over the process ion complexation and release.

Results and Discussion

The synthesis of COF-TMT-BT involves a Brønsted acid-catalyzed aldol condensation between the activated methyl groups of 2,4,6-trimethyl-1,3,5-triazine (TMT) and the aryl aldehydes of 4,4′-(benzothiadiazole-4,7-diyl)dibenzaldehyde (BT) at 150 °C for 72 h (Figure 1a, Figures S1 and S2 and Supporting Information for experimental details). As shown in Figure 1b, the powder X-ray diffraction (PXRD) pattern of COF-TMT-BT reveals that its structure is crystalline, and the pattern matches more precisely with the simulated PXRD of the aligned AA stacked model (Figure 1c) in space group of hexagonal *P*63/*m* as compared with AB stacked model (Figures S3 and S4). The full profile Pawley refinement of the model against the experimental pattern yields a unit cell of $a=b=37.6$ Å, $c=3.7$ Å, $\alpha=\beta=90°$, $\gamma=120°$ with good agreement factors of $R_{wp}=3.93\,\%$ and $R_p=3.08\,\%$ (Table S1, Supporting Information).

The olefin linkage of COF-TMT-BT can be unambiguously confirmed by Fourier transform infrared (FT-IR) spectroscopy and edited solid-state (SS) ^{13}C cross-polarization magic angle spinning (CP-MAS) nuclear magnetic resonance (NMR) spectroscopy. In the FT-IR spectrum (Figure S5, orange spectrum), COF-TMT-BT displays a characteristic peak at 1626 cm^{-1}, which belongs to the C=C stretching of the formed olefin linkage, and it is not present in the starting monomers TMT or BT (Figure S5, black and blue spectra, respectively). In addition, the characteristic peak at 1686 cm^{-1} of the C=O stretching in BT is extensively attenuated in COF-TMT-BT, indicating the successful aldol condensation. The solid-state structure of COFs is then analysed by SS CP-MAS NMP spectroscopy.[28] In the unlabelled COF-TMT-BT (Figure 1d, blue spectrum), the clear and unambiguous assignment of the alkene carbon peaks is not possible due to overlapped signals of aromatic

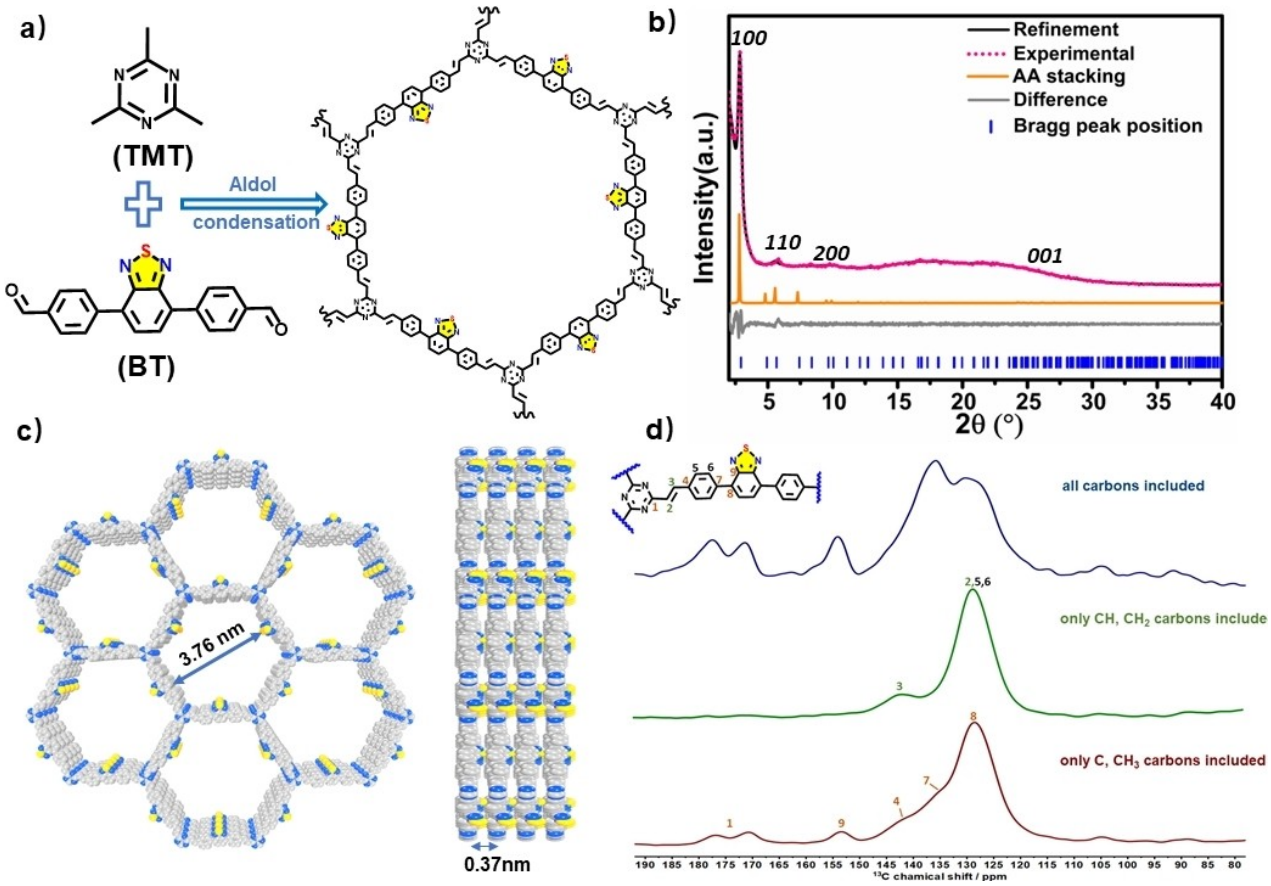

Figure 1. Synthesis and characterization of COF-TMT-BT. a) Illustration of the synthetic route of COF-TMT-BT, b) PXRD pattern fitting of COF-TMT-BT with Pawley refinement and simulated AA-stacking patterns, c) top and side view of the AA eclipsed model, d) edited solid-state ^{13}C NMR spectra of COF-TMT-BT.

and olefinic carbons in the backbone of the structure. Therefore, more precise assignments of the chemical shifts to the expected moieties are obtained by editing ^{13}C CP-MAS NMR spectral.[29] The observed signals located at d ≈142 and 135 ppm can be uniquely attributed to the aromatic carbon signals of vinylene (–CH=CH–) (Figure 1d). The chemical shift signal of the labelled BT aldehyde starting material is observed around 192 ppm and it is largely attenuated in COF TMT-BT (Figure S6). Moreover, the COF-TMT-BT surprisingly reveals two distinct aromatic triazine carbon (C_1) signals at ≈170 and ≈176 ppm which are in good agreement with the reported ^{13}C NMR spectrum of 2,4,6-triamino-1,3,5-triazine (melamine). The different hydrogen-bonding environment results in two chemically diverse carbon atoms and hence in two different signals in the ^{13}C NMR spectrum (Figure 1d).[30]

To gain more insight into the electronic states of sulfur and nitrogen heteroatoms of benzothiadiazole units, X-ray photoelectron spectroscopy analyses (XPS) are performed, confirming the presence of C1s, S2p, and N1s electronic states in COF-TMT-BT (Figure S7). The C1s spectrum of the COF-TMT-BT (Figure 2a) shows the presence of three distinctive peaks, located at 284.5 eV, 285.7 eV, and 286.7 eV, and can be attributed to C–C, C–H (e.g., –CH=CH– chains) and C=N bonding in the benzothiadiazole units, respectively.[31] The N1s spectrum of the COF-TMT-BT (Figure 2b) displays two different N signals which come from two different locations within the repeat unit (one in the triazine unit and the other in the benzothiadiazole unit), with the peak at 399.1 eV being originated from the pyridinic-N in benzothiadiazole unit,[32] and the other peak at higher binding energy (at 400.5 eV) due to the pyrrolic-N core levels in triazine moiety.[33] The high-resolution XPS spectra of S2p (Figure 2c) exhibit a peak at ≈165.2 eV along with a shoulder peak at ≈166.4 eV assigned to the benzothiadiazole $S2p_{3/2}$ and $S2p_{1/2}$, respectively.[34] All the experimental findings from the XPS analysis of COF-TMT-BT are in good agreement with the previous FT-IR and ^{13}C CP-MAS NMR results, further verifying the olefin linkage formation and benzothiadiazole moiety in our COF framework.

The morphology of COF-TMT-BT is investigated by field-emission scanning electron (FE-SEM) and it reveals the presence of spherical nanoparticles with a diameter of ≈500 nm. Furthermore, the energy-dispersive spectroscopy (EDS) elemental mapping images confirm the homogeneous nature of the COF-TMT-BT spherical structures with a uniform distribution of C, N, and S elements (Figure 2d–g). The high-resolution transmission electron microscope (HRTEM) image and selected area electron diffraction

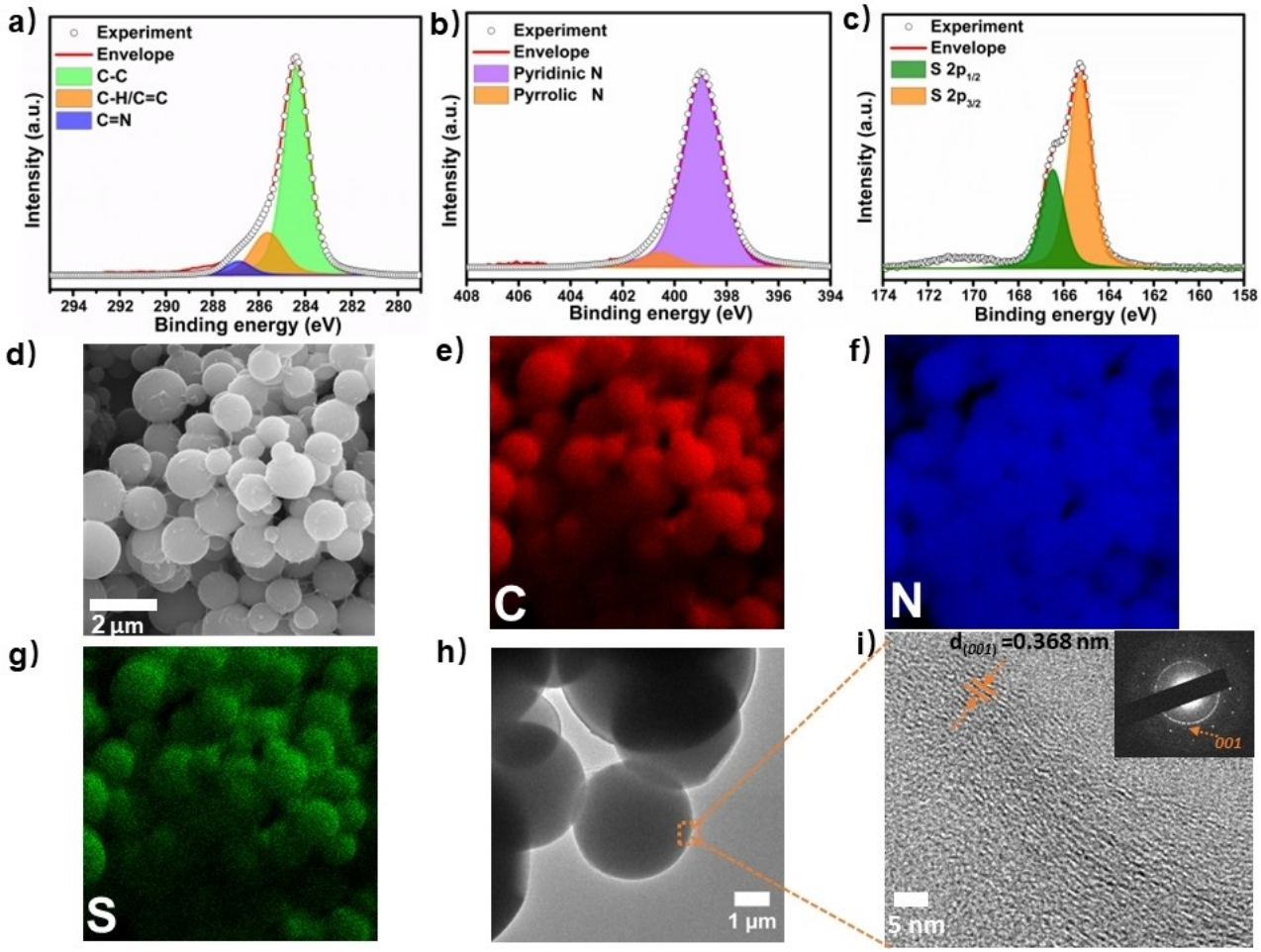

Figure 2. a)–c) High-resolution XPS spectra of COF-TMT-BT for a) C1s, b) N1s, c) S2p, d)–g) FE-SEM image and corresponding elemental mapping analysis for d) SEM, e) EDS map of C, f) EdS map of N, g) EDS map of S, h) TEM images of COF-TMT-BT, i) HR-TEM image and insert SAED pattern (inset) of COF-TMT-BT.

(SAED) pattern (Figure 2h and i) reveal a stacking distance ≈0.37 nm, which is consistent with stacking distance calculated from PXRD analysis in the simulated COF-TMT-BT structure (Figure 1c).

The structural stability of COF-TMT-BT is assessed by thermogravimetric analysis (TGA) and differential scanning calorimetry (DSC) analyses, which reveal high thermal stability up to 450 °C (Figure S9). Furthermore, the porosity and the calculated Brunauer–Emmett–Teller (BET) surface area of COF-TMT-BT are evaluated by N_2 adsorption-desorption isotherms at 77 k (Figure S10 adn S11). As portrayed in Figure S10, COF-TMT-BT exhibits a typical type-II adsorption isotherm along with a high surface area of 342.5 $m^2 g^{-1}$. The pore size distributions (Figure S11) calculated using the non-local density functional theory (NLDFT), show the dominance of micropores of less than 5 nm, in good agreement with the theoretical value (3.76 nm) in AA models (Figure 1c).

The electrochemical performance of COF-TMT-BT in Zn^{2+} storage is assessed in a two-electrode configuration by assembling a COF TMT-BT cathode with a Zn foil anode and 2 M zinctrifluoromethanesulfonate ($Zn(CF_3SO_3)_2$) aqueous electrolyte (Figure 3a). The cyclic voltammograms (CVs) of the first five cycles at 5 $mV s^{-1}$ in the potential range of 0.5–1.6 V *vs* Zn^{2+}/Zn are displayed in Figure 3b. A pair of redox peaks at 1.31 and 1.12 V indicates the reversible insertion/extraction process of Zn^{2+} in the COF structures. Importantly, the peak positions remain almost unchanged during the successive cycling whereas the peak currents gradually increase due to the activation of the COF-TMT-BT cathode. Electrochemical impedance spectroscopy (EIS) is employed to explore the activation of the COF-TMT-BT cathodes, where the charge transfer resistance decreases with the number of charge/discharge cycles (Figure S12). The galvanostatic charge–discharge (GCD) profiles of COF-TMT-BT (Figure 3c) in the explored potential window reveal a high capacity of 283.5, 261.2, 232.6, 191.4, 146.2 mAh g^{-1} at a current density of 0.1, 0.2, 0.5, 1, 2 A g^{-1}, respectively, which are superior to most of the reported cathodes based on COFs or other organic and inorganic electrode materials in aqueous ZIBs (Table S2). Noteworthy, we observe a voltage plateau at 1.27 V using a significantly low current density (i.e., between 0.1 and 0.5 A g^{-1}) for the first time in organic compounds (including

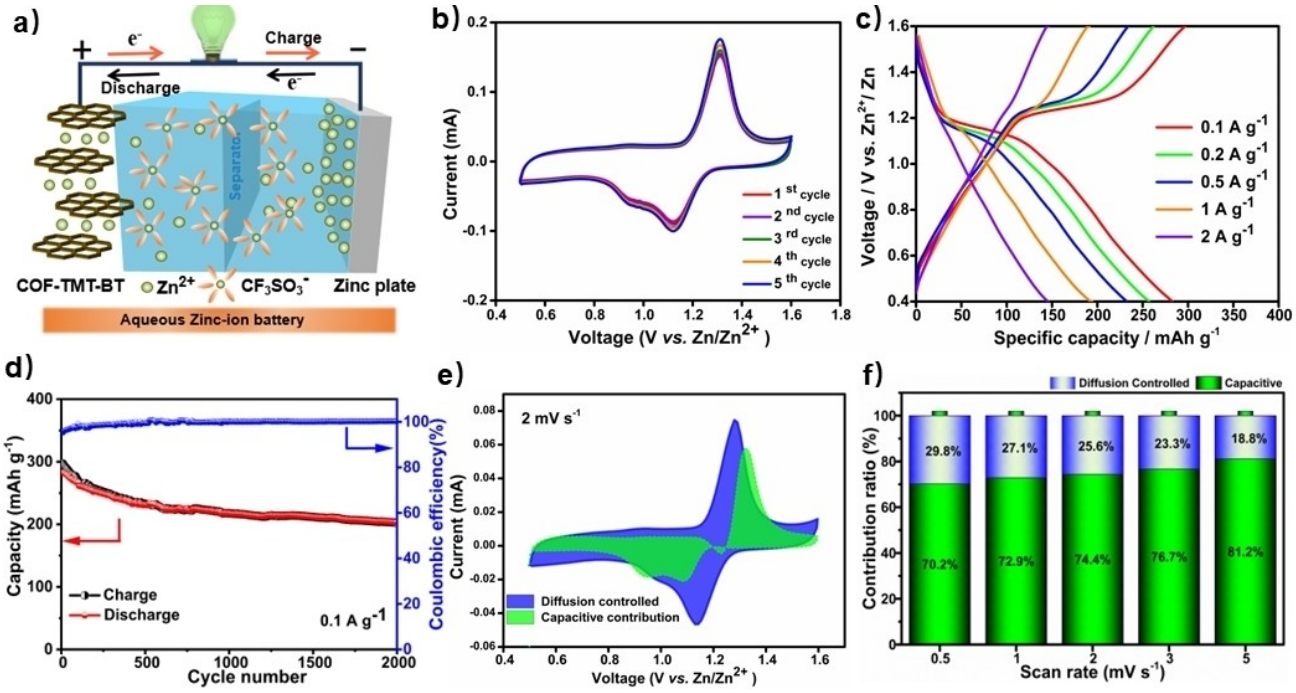

Figure 3. a) Schematic of COF-TMT-BT||$Zn(CF_3SO_3)_2$||Zn energy storage system. used as electrolyte, b) CV curves of COF-TMT-BT at 5 $mV\,s^{-1}$ during 5 cycles, c) GCD profiles for COF-TMT-BT electrodes at various current densities, d) long-term cycling performance at 0.1 $A\,g^{-1}$, e) the comparison of CV curves for the capacitive contribution and diffusion-controlled fraction at 2 $mV\,s^{-1}$, f) capacitive (contribution) and diffusion-controlled contribution of the COF-TMT-BT electrode at different scan rates.

small organic molecules, COFs, and polymers), which is vital for its practical application. The rate capability of COF-TMT-BT is analyzed at different current densities (Figure S13). When the current density decreases from 2 to 0.1 $A\,g^{-1}$, 96.2 % (272.6 $mAh\,g^{-1}$) of the initial specific capacity can be recovered, indicating an excellent rate capability. The long-term cycling test (Figure 3d) shows the high cyclability of COF-TMT-BT electrodes at a current density of 0.1 $A\,g^{-1}$, which can retain a 186.8 $mAh\,g^{-1}$ specific capacity value after 2000 cycles. Moreover, the coulombic efficiency of the COF-TMT-BT cells is well maintained to 99.6 % throughout the 2000 charge–discharge cycles. To ascertain the stability of the electrodes, SEM, energy-dispersive X-ray spectroscopy (EDS) and PXRD analyses of COF-TMT-BT cathode at the pristine electrode and after 2000 cycles are performed (Figure S14–S17). Importantly, the SEM morphology of COF-TMT-BT cathodes after 2000 cycles does not show any obvious change except for the surface doping of a Zn layer, which could indicate their high stability during the charge–discharge process (Figure S16). Remarkably, the ragone plot of COF-TMT-BT-based electrodes (Figure S18) displays an outstanding maximum energy density of 219.6 $Wh\,kg^{-1}$ and power densities of 23.2 $kW\,kg^{-1}$, which is superior to all of the previously reported organic cathode materials in aqueous ZIBs[35] (calculation based on high mass loading of 2.4 $mg\,cm^{-2}$ and the weight ratio of 70 wt % of active material).

To bestow more information on the electrochemical kinetic aspects of COF-TMT-BT cathodes, CV tests at scan rates ranging from 0.5 to 5 $mV\,s^{-1}$ are conducted (Figure S19). The CV curves only exhibit a small peak shift within the scan rate of 0.5–5 $mV\,s^{-1}$, indicating excellent electrochemical reversibility. The electrochemical kinetics COF-TMT-BT are investigated by exploiting the procedure proposed by Wu et al., according to the equation: $I = a\nu^b$, where i represents current density, ν refers to scan rate, a and b are variable parameters.[36] It is well-established that when the b-value is closer to 0.5 means a diffusion-controlled process, while a b-value is closer to 1 indicates a capacitive-controlled process in the charge storage mechanism. The b-values of COF-TMT-BT cathodes calculated from the slope of $\log(i)-\log(\nu)$ curves in Figure S21 amount to 0.71 and 0.76, which indicates that the Zn^{2+} storage mechanism of the COF-TMT-BT cathodes is dominated by a capacitive contribution. To further quantify the capacitive ($k_1\nu$) and diffusion-controlled contribution ($k_2\nu^{0.5}$) from the CV curves at different scan rates, the following equation can be used: $i = k_1\nu + k_2\nu^{0.5}$, where k_1 and k_2 are constants parameters.[37] As shown in Figure S21, the capacitive contribution to the charge storage mechanism for the COF-TMT-BT cathodes is the highest (81.2 %) at the highest scan rate (5 $mV\,s^{-1}$). The capacitive contribution gradually decreases (76.7, 74.4, 72.9 and 70.2 %) at lower scan rates (3, 2, 1 and 0.5 $mV\,s^{-1}$, respectively) (Figure 3e, f, and S21). Thus, the coexistence of capacitive and diffusion-controlled charge storage mechanisms confirms the pseudocapacitive nature of COF-TMT-BT materials which is highly beneficial for energy storage.[15,38]

To shed light onto the charge storage mechanism of Zn^{2+} from the benzothiadiazole electrochemically active units, a series of in situ and ex situ structural and compositional analyses are carried out, including ex situ XPS, in situ FT-IR and ex situ PXRD (the details are provided in Supporting Information).

DFT calculations are performed to simulate the atomic configuration evolution of the COF-TMT-BT cathode during the Zn^{2+} storage process (the calculation details can be found in the Supporting Information). The molecule's electronic structure plays a vital role in determining its redox properties and therefore the structure in Figure S28 is considered as a repetitive unit for the calculations.[39] The simulated projected density of states (PDOS) and band structures are first calculated to elucidate the origin of the interactions from the perspective of the electronic structures. As shown in Figures 4a and b, the monolayer of COF-TMT-BT possesses a narrowed indirect band gap of 1.77 eV, which is reduced to 1.11 eV in the multilayer structure. The narrowing of the band gap reveals an enhanced excitation of charge carriers to the conduction band. The energy levels of the lowest occupied molecular orbital (LUMO) and the highest occupied molecular orbital (HOMO) are used to study the redox properties of the COF-TMT-BT materials (Figure 4c). The HOMO orbital of the COF-TMT-BT unit is primarily distributed on the benzothiadiazole moieties without a continuous delocalization, and also for the LUMO orbital, the electron cloud is mainly localized around the benzothiadiazole units, demonstrating that the benzothiadiazole units possess theoretical good electron affinities and high reduction potential.[40] The electrostatic potential surface is further simulated to verify that benzothiadiazole units are the electrochemically active sites for cation chelation. As shown in Figure 4d, the electronegativity of COF-TMT-BT is located around the orange region near the corner nitrogen of the two neighbouring triazine cores. In addition, the electronegative region unit spreads over the entire boundary within the COF-TMT-BT molecular plane, which indicates the possible active sites for hosting ions in the COF-TMT-BT. The binding energies (BE) of COF-TMT-BT after the redox reaction with Zn^{2+} are calculated at the B3LYP/6-31 + G(d) level by using three possible model compounds (Figure 4e).[41] The optimized structures of Zn_X@COF-TMT-BT ($X=2$, 4, 6) and the average binding energy needed for each Zn^{2+} are displayed in Figure 4e, based on the minimum energy principle. The Zn_6@COF-TMT-BT model shows the most stable configuration after the Zn^{2+} uptake. According to these DFT theoretical calculation results and some previous reports,[42] we propose the following electrochemical mechanism of COF-TMT-BT during the reversible process of Zn^{2+} ion insertion/extraction: COF-TMT-BT stores charges via an ion-coordination process where each Zn^{2+} ion binds, i.e., complexes, the S atoms from the benzothiadiazole units to form S–Zn–S bond in the adjacent COF-TMT-BT layers. To provide insights on the magnitude of the interaction between Zn^{2+} ions and the benzothiadiazole units, a theoretical model is constructed, and the corresponding binding energies are calculated. As shown in Figure S29, when C=N bond and S units co-chelate with Zn^{2+} ions, the Zn^{2+} ions dissociate spontaneously, because the corresponding binding energy, amounting to 3.04 eV, is much higher than the binding energy for Zn^{2+} ions coordinated with S of the adjacent layers' thiadiazole ring forming S–Zn–S, which corresponds to 1.67 eV. Furthermore, the Zn^{2+} insertion in most of ZIBs active materials studied in aqueous electrolytes is usually accompanied with H^+ insertion,[43] which is also monitored in the case of COF-TMT-BT electrode material. To determine the H^+, Zn^{2+} insertion capability of the COF-TMT-BT, a CV test is performed in aqueous electrolyte at different pH as well as in non-aqueous 0.2 M $Zn(CF_3SO_3)_2$/acetonitrile(AN) electrolyte (Figure S30). The CV curves show a single oxidation peak and remain unaffected in all the conditions, confirming that the Zn^{2+} insertion dominates the electrochemical activity of COF-TMT-BT.

To further confirm that benzothiadiazole units play a key role in the Zn^{2+} storage, we performed a control experiment where we synthesized a similar olefin-linked COF without benzothiadiazole moieties (i.e., the BT monomer is replaced by 4,4′-biphenyldicarbaldehyde (BP)), COF-TMT-BP (Figure S31), and we assess its electrochemical performance as cathode material in aqueous ZIBs. The CV test results of the COF-TMT-BP cathode do not exhibit obvious oxidation and reduction peaks in the same potential range of COF-TMT-BT, indicating the absence of Zn^{2+} ion-coordination (Figure S35a). We finally extended the use benzothiadiazole units as electrochemically-active sites in Zn^{2+} energy storage for the fabrication of other COFs with different linkages. Therefore, a further benzothiadiazole-based imine-linked COF is synthesized through a Schiff-base reaction of tris-(4-aminophenyl)triazine (TAT) and BT monomer under solvothermal conditions (the synthesis details can be found in Supporting Information), COF-TAT-BT (Figure S33). Interestingly, the CV analysis of the COF-TAT-BT cathode displays a clear oxidation and reduction peak (Figure S35b), which confirms once again that the benzothiadiazole units are the electrochemically active sites in imine-linked COF for aqueous ZIBs.

Conclusion

In summary, we have synthesized a new olefin-linked, benzothiadiazole-based 2D-COF, i.e. COF-TMT-BT, as suitable novel cathode material for aqueous ZIBs. The benzothiadiazole groups are multifunctional: by design they are both electrochemically-active and contain S and N atoms that can reversibly coordinate Zn^{2+} via controlled ion complexation and release. The as-synthesized COF-TMT-BT, when integrated as cathode material in aqueous ZIBs, delivered a high capacity of 283.5 $mAh\,g^{-1}$ at a current density of 0.1 $A\,g^{-1}$ and an outstanding maximum energy and power densities of 219.6 $Wh\,kg^{-1}$, 23.2 $kW\,kg^{-1}$, respectively, which are superior to most of the reported COFs and another organic or inorganic cathodes materials for aqueous ZIBs. The irreversible covalent C=C linkages, provided COF-TMT-BT with an improved stability in aqueous-based electrolytes, retaining a 186.8 $mAh\,g^{-1}$ specific capacity value

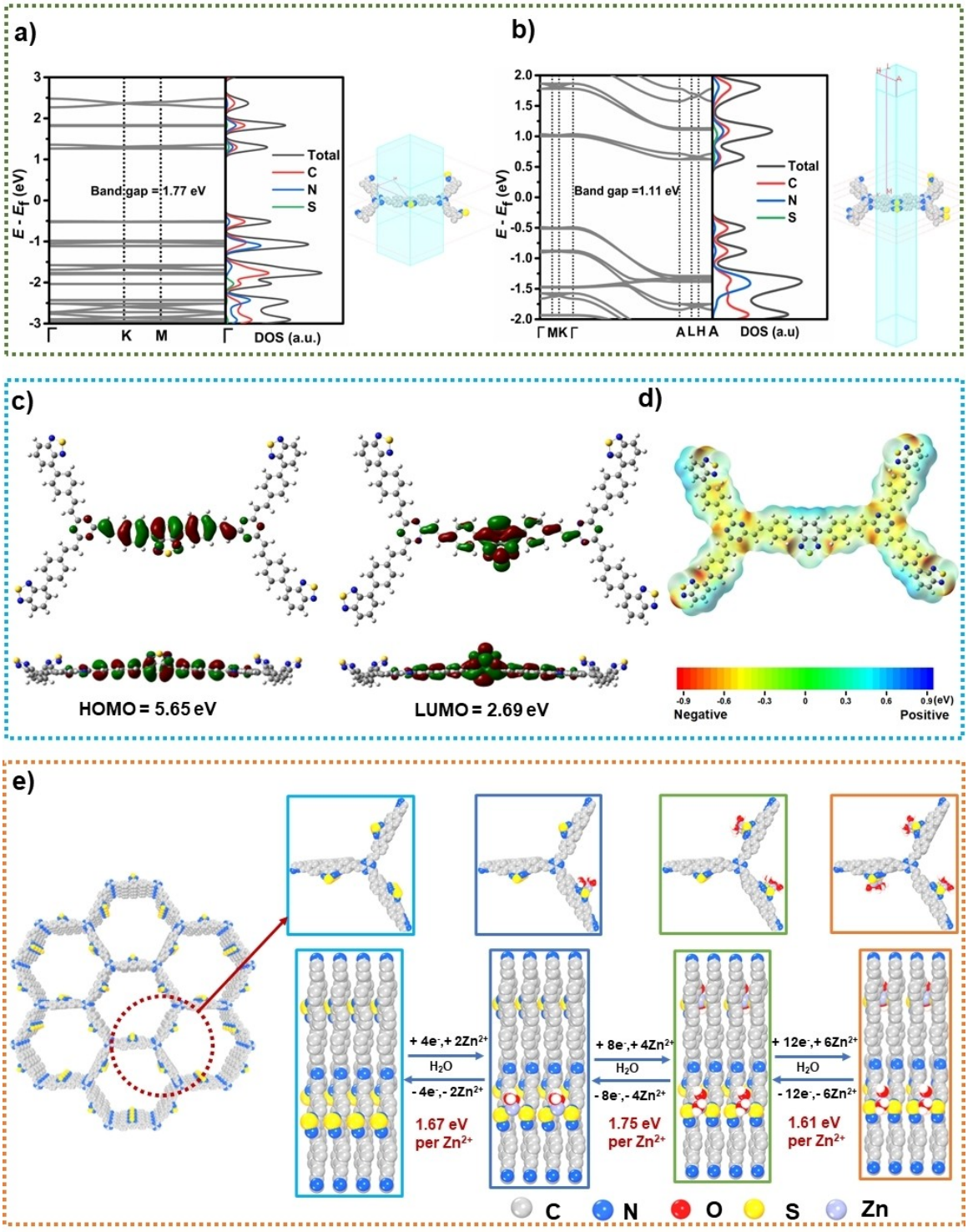

Figure 4. a) Simulated band structure and PDOS of a monolayer COF-TMT-BT with corresponding first Brillouin zone and high symmetry K-points. Γ (0, 0, 0); K (−1/3, 2/3, 0); M (0, 0.5, 0). b) Simulated band structure and PDOS of COF-TMT-BT multilayers with corresponding first Brillouin zone and high symmetry K-points. Γ (0, 0, 0); K (−1/3, 2/3, 0); M (0, 0.5, 0); A (0, 0, 0.5); H (−1/3, 2/3, 0.5); L (0, 0.5, 0.5). c) HOMO and LUMO orbitals of COF-TMT-BT repetitive unit. d) Electrostatic potential surface of COF-TMT-BT repetitive units. e) Binding energy for COF-TMT-BT at each zincation stage (H atom deleted for clarity).

after 800 cycles. We believe that our new benzothiadiazole functionalized 2D olefin-linked COF-TMT-BT not only paves the way for the further rational design of benzothiadiazole-based COF electrodes but also broadens the applications of COFs in aqueous ZIBs.

Acknowledgements

We acknowledge the financial support from the European Commission through the Marie Sklodowska-Curie project ULTIMATE (GA-813036), the Interdisciplinary Thematic Institute SysChem via the IdEx Unistra (ANR-10-IDEX-0002) within the program Investissement d'Avenir program, the International Center for Frontier Research in Chemistry (icFRC), the Institut Universitaire de France (IUF), Chinese Scholarship Council, and the National Science Centre (grant no. 2020/36/C/ST5/00247). The authors thank D.Sc. Michal Bielejewski from the Institute of Molecular Physics Polish Academy of Sciences for the high-resolution solid-state NMR data, and Dr.Cyril Antheaume for the MALDI-TOF mass spectrometry analysis.

Conflict of Interest

The authors declare no conflict of interest.

Data Availability Statement

The data that support the findings of this study are available from the corresponding author upon reasonable request.

Keywords: Charge Storage Mechanism · Covalent Organic Frameworks · Energy Storage Devices · Functional Porous Materials · Zinc-Ion Batteries

[1] a) M. Song, H. Tan, D. Chao, H. J. Fan, *Adv. Funct. Mater.* **2018**, *28*, 1802564; b) N. Zhang, X. Chen, M. Yu, Z. Niu, F. Cheng, J. Chen, *Chem. Soc. Rev.* **2020**, *49*, 4203–4219; c) M. Zhang, R. Liang, T. Or, Y. P. Deng, A. Yu, Z. Chen, *Small Struct.* **2021**, *2*, 2000064; d) P. Ruan, S. Liang, B. Lu, H. J. Fan, J. Zhou, *Angew. Chem. Int. Ed.* **2022**, *61*, e202200598; *Angew. Chem.* **2022**, *134*, e202200598.

[2] a) D. Kundu, B. D. Adams, V. Duffort, S. H. Vajargah, L. F. Nazar, *Nat. Energy* **2016**, *1*, 16119; b) H. Geng, M. Cheng, B. Wang, Y. Yang, Y. Zhang, C. C. Li, *Adv. Funct. Mater.* **2020**, *30*, 1907684; c) B. Deka Boruah, A. Mathieson, S. K. Park, X. Zhang, B. Wen, L. Tan, A. Boies, M. De Volder, *Adv. Energy Mater.* **2021**, *11*, 2100115.

[3] a) Y. Zeng, X. Zhang, Y. Meng, M. Yu, J. Yi, Y. Wu, X. Lu, Y. Tong, *Adv. Mater.* **2017**, *29*, 1700274; b) X. Zhang, S. Wu, S. Deng, W. Wu, Y. Zeng, X. Xia, G. Pan, Y. Tong, X. Lu, *Small Methods* **2019**, *3*, 1900525; c) S. Gao, B. Li, H. Tan, F. Xia, O. Dahunsi, W. Xu, Y. Liu, R. Wang, Y. Cheng, *Adv. Mater.* **2022**, *34*, 2201510.

[4] a) X. He, H. Zhang, X. Zhao, P. Zhang, M. Chen, Z. Zheng, Z. Han, T. Zhu, Y. Tong, X. Lu, *Adv. Sci.* **2019**, *6*, 1900151; b) Y. Liu, J. Wang, Y. Zeng, J. Liu, X. Liu, X. Lu, *Small* **2020**, *16*, 1907458.

[5] a) Z. Liu, G. Pulletikurthi, F. Endres, *ACS Appl. Mater. Interfaces* **2016**, *8*, 12158–12164; b) X. Liu, J. Han, J. Deng, S. Imhanria, Z. Ren, W. Wang, *J. Alloys Compd.* **2020**, *832*, 154896.

[6] a) T. Sun, J. Xie, W. Guo, D. S. Li, Q. Zhang, *Adv. Energy Mater.* **2020**, *10*, 1904199; b) T. Zhang, Y. Tang, G. Fang, C. Zhang, H. Zhang, X. Guo, X. Cao, J. Zhou, A. Pan, S. Liang, *Adv. Funct. Mater.* **2020**, *30*, 2002711; c) D. Chao, W. Zhou, F. Xie, C. Ye, H. Li, M. Jaroniec, S.-Z. Qiao, *Sci. Adv.* **2020**, *6*, eaba4098; d) H. He, J. Lian, C. Chen, Q. Xiong, C. C. Li, M. Zhang, *Nano-Micro Lett.* **2022**, *14*, 106.

[7] a) A. P. Côté, A. I. Benin, N. W. Ockwig, M. O'Keeffe, A. J. Matzger, OmarM. Yaghi, *Science* **2005**, *310*, 1166–1170; b) X. Feng, X. Ding, D. Jiang, *Chem. Soc. Rev.* **2012**, *41*, 6010–6022; c) C. S. Diercks, O. M. Yaghi, *Science* **2017**, *355*, eaal1585; d) D. Rodríguez-San-Miguel, F. Zamora, *Chem. Soc. Rev.* **2019**, *48*, 4375–4386.

[8] K. Zhang, K. O. Kirlikovali, R. S. Varma, Z. Jin, H. W. Jang, O. K. Farha, M. Shokouhimehr, *ACS Appl. Mater. Interfaces* **2020**, *12*, 27821–27852.

[9] a) D. G. Wang, T. Qiu, W. Guo, Z. Liang, H. Tabassum, D. Xia, R. Zou, *Energy Environ. Sci.* **2021**, *14*, 688–728; b) E. Vitaku, C. N. Gannett, K. L. Carpenter, L. Shen, H. D. Abruña, W. R. Dichtel, *J. Am. Chem. Soc.* **2020**, *142*, 16–20.

[10] a) R. Shi, L. Liu, Y. Lu, C. Wang, Y. Li, L. Li, Z. Yan, J. Chen, *Nat. Commun.* **2020**, *11*, 178; b) Y. Cao, M. Wang, H. Wang, C. Han, F. Pan, J. Sun, *Adv. Energy Mater.* **2022**, *12*, 2200057; c) S. Kandambeth, V. S. Kale, O. Shekhah, H. N. Alshareef, M. Eddaoudi, *Adv. Energy Mater.* **2022**, *12*, 2100177; d) D. Pakulski, V. Montes-García, A. Gorczyński, W. Czepa, T. Chudziak, P. Samorì, A. Ciesielski, *J. Mater. Chem. A* **2022**, *10*, 16685–16696.

[11] A. Khayum M, M. Ghosh, V. Vijayakumar, A. Halder, M. Nurhuda, S. Kumar, M. Addicoat, S. Kurungot, R. Banerjee, *Chem. Sci.* **2019**, *10*, 8889–8894.

[12] M. Yu, N. Chandrasekhar, R. K. M. Raghupathy, K. H. Ly, H. Zhang, E. Dmitrieva, C. Liang, X. Lu, T. D. Kühne, H. Mirhosseini, I. M. Weidinger, X. Feng, *J. Am. Chem. Soc.* **2020**, *142*, 19570–19578.

[13] S. Zheng, D. Shi, D. Yan, Q. Wang, T. Sun, T. Ma, L. Li, D. He, Z. Tao, J. Chen, *Angew. Chem. Int. Ed.* **2022**, *61*, e202117511; *Angew. Chem.* **2022**, *134*, e202117511.

[14] a) W. Wang, V. S. Kale, Z. Cao, S. Kandambeth, W. Zhang, J. Ming, P. T. Parvatkar, E. Abou-Hamad, O. Shekhah, L. Cavallo, M. Eddaoudi, H. N. Alshareef, *ACS Energy Lett.* **2020**, *5*, 2256–2264; b) W. Wang, V. S. Kale, Z. Cao, Y. Lei, S. Kandambeth, G. Zou, Y. Zhu, E. Abouhamad, O. Shekhah, L. Cavallo, M. Eddaoudi, H. N. Alshareef, *Adv. Mater.* **2021**, *33*, 2103617.

[15] X. Yue, H. Liu, P. Liu, *Chem. Commun.* **2019**, *55*, 1647–1650.

[16] C. Zhang, W. Ma, C. Han, L. W. Luo, A. Daniyar, S. Xiang, X. Wu, X. Ji, J.-X. Jiang, *Energy Environ. Sci.* **2021**, *14*, 462–472.

[17] Z. Lin, H. Y. Shi, L. Lin, X. Yang, W. Wu, X. Sun, *Nat. Commun.* **2021**, *12*, 4424.

[18] Q. Zhao, W. Huang, Z. Luo, L. Liu, Y. Lu, Y. Li, L. Li, J. Hu, H. Ma, J. Chen, *Sci. Adv.* **2018**, *4*, eaao1761.

[19] K. W. Nam, H. Kim, Y. Beldjoudi, T. W. Kwon, D. J. Kim, J. F. Stoddart, *J. Am. Chem. Soc.* **2020**, *142*, 2541–2548.

[20] Y. Wang, C. Wang, Z. Ni, Y. Gu, B. Wang, Z. Guo, Z. Wang, D. Bin, J. Ma, Y. Wang, *Adv. Mater.* **2020**, *32*, 2000338.

[21] D. Kundu, P. Oberholzer, C. Glaros, A. Bouzid, E. Tervoort, A. Pasquarello, M. Niederberger, *Chem. Mater.* **2018**, *30*, 3874–3881.

[22] N. Wang, Z. Guo, Z. Ni, J. Xu, X. Qiu, J. Ma, P. Wei, Y. Wang, *Angew. Chem. Int. Ed.* **2021**, *60*, 20826–20832; *Angew. Chem.* **2021**, *133*, 20994–21000.

[23] a) H. G. Wang, X. B. Zhang, *Chem. Eur. J.* **2018**, *24*, 18235–18245; b) S. Y. An, T. B. Schon, B. T. McAllister, D. S. Seferos, *EcoMat* **2020**, *2*, e12055.

[24] S. Xu, G. Wang, B. P. Biswal, M. Addicoat, S. Paasch, W. Sheng, X. Zhuang, E. Brunner, T. Heine, R. Berger, X. Feng, *Angew. Chem. Int. Ed.* **2019**, *58*, 849–853; *Angew. Chem.* **2019**, *131*, 859–863.

[25] T. Shimizu, H. Wang, D. Matsumura, K. Mitsuhara, T. Ohta, H. Yoshikawa, *ChemSusChem* **2020**, *13*, 2256–2263.
[26] J. Gao, M. A. Lowe, S. Conte, S. E. Burkhardt, H. D. Abruña, *Chem. Eur. J.* **2012**, *18*, 8521–8526.
[27] a) M. Li, C. An, W. Pisula, K. Müllen, *Acc. Chem. Res.* **2018**, *51*, 1196–1205; b) H. N. Tsao, D. M. Cho, I. Park, M. R. Hansen, A. Mavrinskiy, D. Y. Yoon, R. Graf, W. Pisula, H. W. Spiess, K. Müllen, *J. Am. Chem. Soc.* **2011**, *133*, 2605–2612; c) M. Zhang, H. N. Tsao, W. Pisula, C. Yang, A. K. Mishra, K. Müllen, *J. Am. Chem. Soc.* **2007**, *129*, 3472–3473.
[28] a) C. Yuan, S. Fu, K. Yang, B. Hou, Y. Liu, J. Jiang, Y. Cui, *J. Am. Chem. Soc.* **2021**, *143*, 369–381; b) H. Lyu, C. S. Diercks, C. Zhu, O. M. Yaghi, *J. Am. Chem. Soc.* **2019**, *141*, 6848–6852.
[29] X. L. Wu, K. W. Zilm, *J. Magn. Reson. Ser. A* **1993**, *102*, 205–213.
[30] B. Jürgens, E. Irran, J. Senker, P. Kroll, H. Müller, W. Schnick, *J. Am. Chem. Soc.* **2003**, *125*, 10288–10300.
[31] a) A. R. b. Mohd Yusoff, H. P. Kim, J. Jang, *Nanoscale* **2014**, *6*, 1537–1544; b) M. Mohammadnezhad, B. Aïssa, C. Harnagea, F. Rosei, *J. Electrochem. Soc.* **2020**, *167*, 136504.
[32] a) S. Cho, J. H. Seo, S. H. Park, S. Beaupré, M. Leclerc, A. J. Heeger, *Adv. Mater.* **2010**, *22*, 1253–1257; b) P. Jha, S. P. Koiry, V. Saxena, P. Veerender, A. Gusain, A. K. Chauhan, A. K. Debnath, D. K. Aswal, S. K. Gupta, *Org. Electron.* **2013**, *14*, 2635–2644.
[33] a) D. Y. Osadchii, A. I. Olivos-Suarez, A. V. Bavykina, J. Gascon, *Langmuir* **2017**, *33*, 14278–14285; b) R. Xue, H. Gou, L. Zhang, Y. Liu, H. Rao, G. Zhao, *New J. Chem.* **2021**, *45*, 679–684.
[34] a) D. G. Castner, K. Hinds, D. W. Grainger, *Langmuir* **1996**, *12*, 5083–5086; b) J. S. Kim, P. K. H. Ho, C. E. Murphy, R. H. Friend, *Macromolecules* **2004**, *37*, 2861–2871.
[35] Z. Guo, Y. Ma, X. Dong, J. Huang, Y. Wang, Y. Xia, *Angew. Chem. Int. Ed.* **2018**, *57*, 11737–11741; *Angew. Chem.* **2018**, *130*, 11911–11915.
[36] a) J. Wang, J. Polleux, J. Lim, B. Dunn, *J. Phys. Chem. C* **2007**, *111*, 14925–14931; b) Y. Jin, L. Zou, L. Liu, M. H. Engelhard, R. L. Patel, Z. Nie, K. S. Han, Y. Shao, C. Wang, J. Zhu, H. Pan, J. Liu, *Adv. Mater.* **2019**, *31*, 1900567.
[37] H. S. Kim, J. B. Cook, H. Lin, Jesse S. Ko, Sarah H. Tolbert, V. Ozolins, B. Dunn, *Nat. Mater.* **2017**, *16*, 454–460.
[38] a) H. Y. Shi, Y. J. Ye, K. Liu, Y. Song, X. Sun, *Angew. Chem. Int. Ed.* **2018**, *57*, 16359–16363; *Angew. Chem.* **2018**, *130*, 16597–16601; b) N. Wang, X. Dong, B. Wang, Z. Guo, Z. Wang, R. Wang, X. Qiu, Y. Wang, *Angew. Chem. Int. Ed.* **2020**, *59*, 14577–14583; *Angew. Chem.* **2020**, *132*, 14685–14691; c) Z. Tie, L. Liu, S. Deng, D. Zhao, Z. Niu, *Angew. Chem. Int. Ed.* **2020**, *59*, 4920–4924; *Angew. Chem.* **2020**, *132*, 4950–4954.
[39] J. C. Bachman, R. Kavian, D. J. Graham, D. Y. Kim, S. Noda, D. G. Nocera, Y. Shao-Horn, S. W. Lee, *Nat. Commun.* **2015**, *6*, 7040.
[40] a) C. Peng, G. H. Ning, J. Su, G. Zhong, W. Tang, B. Tian, C. Su, D. Yu, L. Zu, J. Yang, M. F. Ng, Y. S. Hu, Y. Yang, M. Armand, K. P. Loh, *Nat. Energy* **2017**, *2*, 17074; b) C. Cui, X. Ji, P. F. Wang, G. L. Xu, L. Chen, J. Chen, H. Kim, Y. Ren, F. Chen, C. Yang, X. Fan, C. Luo, K. Amine, C. Wang, *ACS Energy Lett.* **2020**, *5*, 224–231.
[41] a) V. A. Rassolov, J. A. Pople, M. A. Ratner, T. L. Windus, *J. Chem. Phys.* **1998**, *109*, 1223–1229; b) K. C. Kim, T. Liu, S. W. Lee, S. S. Jang, *J. Am. Chem. Soc.* **2016**, *138*, 2374–2382; c) D. Ma, H. Zhao, F. Cao, H. Zhao, J. Li, L. Wang, K. Liu, *Chem. Sci.* **2022**, *13*, 2385–2390.
[42] a) Y. Liang, Y. Jing, S. Gheytani, K. Y. Lee, P. Liu, A. Facchetti, Y. Yao, *Nat. Mater.* **2017**, *16*, 841–848; b) Z. Guo, Y. Ma, X. Dong, J. Huang, Y. Wang, Y. Xia, *Angew. Chem. Int. Ed.* **2018**, *57*, 11737–11741; *Angew. Chem.* **2018**, *130*, 11911–11915.
[43] a) S. Zheng, D. Shi, D. Yan, Q. Wang, T. Sun, T. Ma, L. Li, D. He, Z. Tao, J. Chen, *Angew. Chem. Int. Ed.* **2022**, *61*, e202117511; *Angew. Chem.* **2022**, *134*, e202117511; b) T. Sun, W. Zhang, Q. Nian, Z. Tao, *Chem. Eng. J.* **2023**, *452*, 139324; c) D. Han, T. Sun, H. Du, Q. Wang, S. Zheng, T. Ma, Z. Tao, *Batteries Supercaps* **2022**, *5*, e202200219.

Manuscript received: November 2, 2022
Accepted manuscript online: January 10, 2023
Version of record online: January 25, 2023